

2 Superior removal of As(III) and As(V) from water with Mn-doped β -

3 FeOOH nanospindles on carbon foam

4 Bing Yan ^{1,3*}, Tian Liang ², Xiaohui Yang ² □ Ashok J. Gadgil ^{3*}

5 -----
6 ¹ School of Environmental Studies, China University of Geosciences, Wuhan 430074, PR China

7 ² Faculty of materials science and chemistry, China University of Geosciences, Wuhan 430074, PR

8 China

9 ³ Department of Civil and Environmental Engineering, University of California, Berkeley, CA 94720-

10 1710, USA

11 * Corresponding author E-mail: yanbing@cug.edu.cn

12 * Co-corresponding author E-mail: ajgadgil@berkeley.edu

13 14 **Abstract:**

15 Arsenic pollution of water is one of the severest environmental challenges threatening human health.

16 Iron-based nanomaterials have been demonstrated effective in arsenic removal. However, they generally

17 suffer from low removal efficiency towards highly toxic As(III), loss of active sites owing to

18 agglomeration, and poor reusability. Herein, we report a carbonized melamine foam supported Mn(IV)-

19 doped β -FeOOH nanospindles(CF@Mn-FeOOH NSp) for tackling the technical hurdles. The designed

20 CF@Mn-FeOOH NSp appears as a free-standing monolith through a low-cost and straightforward

21 hydrothermal method. The atomic-scale integration of Mn(IV) into β -FeOOH enables an *oxidation-*

22 *adsorption* bifunctionality, where Mn(IV) serves as oxidizer for As(III) and Fe(III) acts as adsorber for

23 As(V). The maximal adsorption capacity for As(V) and As(III) can reach 152 and 107 mg g⁻¹,
24 respectively. Meanwhile, As in simulated high arsenic groundwater can be decreased to below 10 µg L⁻¹
25 within 24 h. By simple “filtrating-washing”, 85% and 82% of its initial adsorption capacity for As(V)
26 and As(III) can be easily recovered even after 5-cycles reuse. Kinetics and isotherm adsorption study
27 indicate that the arsenic adsorption behavior is mainly through chemical bonding during single-layer
28 adsorbing process. The as-prepared CF@Mn-FeOOH offers a scalable, efficient, and recyclable solution
29 for arsenic removal in groundwater and wastewater from mines and industry.

30 **Keywords:** arsenic removal; monolith; manganese doping; FeOOH; oxidation-adsorption

31 **1. Introduction**

32 The maximum contaminant limit of arsenic in drinking water proposed by World Health
33 Organization (WHO-MCL) is 10 µg L⁻¹ [1, 2]. However, high arsenic contamination of groundwater
34 used for drinking is widely distributed worldwide [3, 4]. The inappropriate disposal of arsenic
35 wastewater from mines and industry (usually at concentrations of tens of mg L⁻¹ and mainly as As(III))
36 continues to contaminate the drinking water [5, 6]. Therefore, it is extremely important and urgent to
37 develop an effective technology to reduce arsenic concentration.

38 Numerous technologies, including adsorption [7], coagulation-precipitation [8], biological
39 degradation [9, 10], and ion exchange [11] are currently applied to remove arsenic from water.
40 Adsorption, owing to its ease of operation, low-cost, high treatment efficiency, and low secondary
41 pollution [12], is considered as one of the most attractive approaches. FeOOH is the mostly studied
42 adsorber for arsenic in water for its excellent adsorption capacity towards arsenate (As(V)) [13-15].
43 However, FeOOH has limited ability to remove arsenite (As(III)), which is 60 times toxicity higher than
44 As(V) [16, 17]. Thus, external oxidants are often utilized to transform As(III) to less-toxic As(V) for

45 subsequent capture and removal by FeOOH in application. Since As(III) is the predominant As species
46 in many areas of high arsenic groundwater [18, 19], adding oxidants in groundwater remediation will
47 inevitably change the water environment and cause secondary pollution [20]. Therefore, to synthesize
48 iron-manganese binary oxide with dual function of “oxidation-adsorption” is usually adopted to solve
49 this problem, where Mn plays as an intrinsic oxidant to oxidize As(III) to As(V) [17, 21-23], which can
50 be more readily adsorbed on the neighboring FeOOH. This *in-situ* process avoids the secondary
51 pollution caused by the addition of external oxidants. However, Mn, Fe, and O cannot be distributed
52 evenly in iron-manganese binary oxide materials prepared via traditional methods (physical mixing or
53 co-precipitation), which leads to partial shielding between active sites and results in inferior arsenic
54 removal performance [24].

55 Atomic-scale doping of Mn(IV) into the FeOOH lattice can effectively expose active sites and
56 facilitate the *in-situ* “oxidation-adsorption”, contributing to a high performance of As adsorption [24,
57 25]. In light of this, a hydrothermal preparation of Mn-doped β -FeOOH (Mn-FeOOH) was proposed.
58 The atomic-scale doping can construct a single-phase Mn(IV)-FeOOH nanospindles, which promotes
59 the homogeneous distribution of the dual active center of “oxidation Mn(IV)-adsorption Fe(III)”,
60 maximizing its arsenic oxidation and adsorption capability. Further, considering the common
61 drawbacks of agglomeration and recycling difficulty as nanomaterial, the macroscopic porous scaffold
62 of oxidized carbon foam are adopted to support nano-adsorbent of Mn(IV)-FeOOH nanospindles,
63 which enables the composite to be recycled easily through a facile “filtrating-washing” process,
64 overcoming the drawback of conventional powdered Mn(IV)-FeOOH nanomaterial [26]. Besides, the
65 carbon foam is derived from the melamine foam (MF), which is a kind of commercial polymer that has
66 low cost, high flexibility, and large-scale availability. At the same time, the porous structure of the

67 scaffold provides plentiful channels for the mass transportation of As(III) to the dual-centers (oxidation
68 Mn(IV)-adsorption Fe(III)), enhancing the adsorbing kinetics of As.

69 In this study, we propose the hydrothermal preparation of a free-standing composite of Mn-FeOOH
70 assembled on oxidized carbon foam (CF@Mn-FeOOH), which exhibits excellent adsorbing capacity
71 towards both As(V) and As(III). Using dosage as 0.5 g L^{-1} , it can reduce As(III) and As(V) from 1 mg
72 L^{-1} to below $10 \text{ }\mu\text{g L}^{-1}$ (WHO-MCL) within 24 h and 12 h, respectively, exceeding the most common
73 iron-based adsorbents [16, 17, 21-24, 27-33]. The raw materials used for preparing the composite are
74 all inexpensive and readily available ($\$12 \text{ kg}^{-1}$ for MF), along with the straightforward preparing method
75 and efficient arsenic adsorption performance, enabling CF@Mn-FeOOH to be a promising candidate
76 for commercial application of arsenic removal.

77

78 **2. Materials and Methods**

79 **2.1 Materials**

80 All chemicals used in this study were of analytical grade (Sinopharm Chemical Reagent Co., Ltd.,
81 China). Arsenic solutions were prepared by dissolving Na_2HAsO_4 and NaAsO_2 in deionized water,
82 respectively. MF was provided by Kelinmei Company in China.

83 **2.2 Synthesis of CF@Mn-FeOOH nanospindles**

84 Carbon foam(CF) was derived from melamine foam (MF) via carbonization under N_2 (at $700 \text{ }^\circ\text{C}$ for 2
85 h, using a temperature ramp of $5 \text{ }^\circ\text{C min}^{-1}$), and cutted into slabs ($3 \times 1.5 \times 0.5 \text{ cm}^3$). The CF pieces were
86 then acidized by $3 \text{ mol L}^{-1} \text{ H}_2\text{SO}_4$ and heated at $120 \text{ }^\circ\text{C}$ for 1 h respectively. After that, the slabs were
87 washed and dried ($T= 50 \text{ }^\circ\text{C}$) to acquire the oxidized CF.

88 Mn-FeOOH nanospindles was obtained by hydrothermal process in stock solution of 10.8 mmol
89 $\text{FeCl}_3 \cdot 6\text{H}_2\text{O}$ (2.92 g), $0.54 \text{ mmol MnCl}_2 \cdot 4\text{H}_2\text{O}$ (0.1068 g , 5% of the iron molar ratio) , 32 mmol NaNO_3

90 (2.72 g), 0.1 mL HCl (37.5 wt%), 9.5 mL deionized water and 22.4 mL acetonitrile (C_2H_3N , >99%).
91 Then the oxidized CF was put into the above solution and stirred for another 60 min and heated at 100
92 °C for 4 h to prepare CF@Mn-FeOOH NSp. A batch of CF@FeOOH NSps was separately prepared
93 according to the above procedures without $MnCl_2 \cdot 4H_2O$.

94 **2.3 Characterization**

95 The crystalline mineral composition was measured by X-ray diffraction (XRD, Bruker D8-FOCUS
96 powder diffraction system). A Fourier transform infrared (FTIR) spectrometer (Nicolet iS50) in the
97 range of 400-4,000 cm^{-1} by means of the KBr pellet technique was used to record the FTIR spectra.
98 Zeta potentials of the samples were measured by a Zeta potential analyzer (Nano ZS90, UK). Thermo
99 Fisher ESCALAB 250Xi XPS was utilized for X-ray photoelectron spectroscopy (XPS). The
100 morphology and nanostructure of the obtained samples were examined using field-emission scanning
101 electron microscope (FE-SEM, Hitachi SU8010 at 10.0 kV). The Brunauer-Emmett-Teller (BET)
102 specific surface area was measured using Micromeritics ASAP 2046 Analyzer, while the pore size
103 distributions of the samples were calculated by adopting the Barrett-Joyner-Halenda (BJH) model.

104 **2.4 Batch adsorption experiments**

105 Batch adsorption experiments were performed at fixed temperature of 25 °C, with 0.5 $g L^{-1}$ adsorbent
106 dosage to study the effects of pH, reaction time, initial concentration of arsenic and co-existing
107 competing anions on arsenic removal in synthetic As(V) and As(III) solution respectively. Suspension
108 samples were adjusted to certain pH by using diluted HCl and NaOH solution (0.1 $mol L^{-1}$).

109 Adsorption isotherm experiments were carried out to determine the arsenic adsorption capacities of
110 adsorbents in As(V) and As(III) solution with initial concentrations ranged from 1-500 $mg L^{-1}$ at pH =7.
111 The adsorption kinetics were studied at pH=7 for 24 h in 20 mL of 10 $mg L^{-1}$ either As(V) or As(III)
112 solution. To determine the effect of initial pH on arsenic removal, 0.5 $g L^{-1}$ of adsorbent was introduced

113 into arsenic solutions (with 20 mg L⁻¹ of either As(III) or As(V)) for 24 h with different initial pH,
114 which were adjusted to 2, 4, 6, 7, 8 and 10 respectively. The influences of co-existing competing anions
115 as Cl⁻ (NaCl, 99.5%), HCO₃⁻ (NaHCO₃, >99%), SO₄²⁻ (Na₂SO₄·10H₂O, >99%) and PO₄³⁻ (NaH₂PO₄, 99.5%)
116 on arsenic adsorption were investigated at two ion concentrations (0.1 and 1 mmol L⁻¹) in 10 mg L⁻¹ of
117 either As(V) or As(III) solution.

118 The high concentrations of soluble As (>1 mg L⁻¹) were measured using inductively coupled plasma
119 atomic emission spectrometry (ICP-AES), while the low concentrations (<1 mg L⁻¹) were determined
120 by atomic fluorescence spectrometry (AFS). Aqueous As(V) and As(III) were separated by filtering the
121 filtrate with As-speciation anion exchange cartridges[34, 35] before testing.

122 **2.5 Oxidation-adsorption mechanism of CF@Mn-FeOOH study**

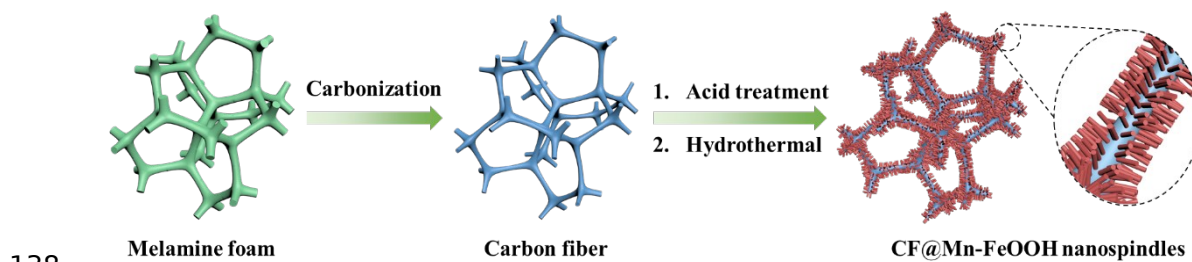
123 In order to explore the function of Mn and Fe-OOH, and unravel the ‘oxidation-adsorption’
124 mechanism of the adsorbent, CF@Mn-FeOOH and CF@FeOOH were compared in the above batch
125 experiments respectively. At the same time, lower concentration of As(III) and As(V) (1 mg L⁻¹), similar
126 to geogenic high arsenic groundwater, were adopted to evaluate the feasibility for potential realistic
127 application. To further clarify the adsorption mechanism of CF@Mn-FeOOH, As speciation in the
128 residual solution was separated to As(III) and As(V) before AFS analysis [36].

129 **2.6 Desorption and reusability experiment**

130 To verify the reusability of the as-obtained materials for arsenic adsorption, the adsorbent was
131 subjected to a five-cycle adsorption-desorption experiment with the same experimental parameters as
132 described in **section 2.4** in 10 mg L⁻¹ of either As(V) or As(III) solution. After each adsorption cycle,
133 the adsorbent was filtered, washed with NaOH solution (0.1 mol L⁻¹) for 30 min, then rinsed with
134 deionized water, soaked in H₂SO₄ solution (0.05 mol L⁻¹) for 10 min, followed by washing and drying
135 before reuse.

136

137 3. Results and discussion

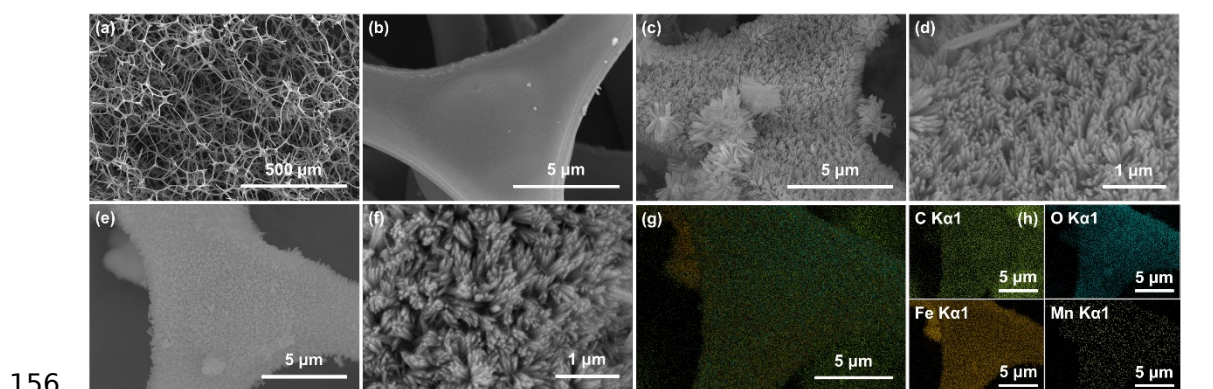


139 **Figure 1.** Schematic illustration for the synthesis of CF@Mn-FeOOH nanospindles.

140 The preparation process is displayed in Figure 1. MF was first carbonized under N_2 . After calcination,
141 MF turned from white to black, with its volume shrank as well as a mass loss of 81.3%, owing to the
142 thermal decomposition of the polymer. Since the thermolysis CF was hydrophobic, an acid pre-
143 oxidation was further carried out to increase the hydrophilicity for the successive loading of FeOOH
144 nanospindles. The objective of this process was to generate abundant oxygen-containing functional
145 groups (such as carboxyl radical) on the CF [26], which are beneficial to the complexation between
146 oxidized CF and metal ions (Fe^{3+} and Mn^{2+}). Subsequently, various reagents ($FeCl_3 \cdot 6H_2O$, $MnCl_2 \cdot 4H_2O$,
147 $NaNO_3$, HCl, deionized water, and acetonitrile) were subjected to a hydrothermal reaction to assemble
148 Mn doped FeOOH nanospindles onto the oxidized CF. During the hydrothermal process, the acidic
149 environment forced Fe^{3+} to hydrolyze and homogeneously precipitate β -FeOOH [37] on the
150 complexation sites along the oxidized CF. Mn(II) was introduced and precipitated with β -FeOOH
151 simultaneously as Mn-FeOOH, which then chemically anchored to CF, generating CF@Mn-FeOOH
152 nanospindles [38]. After hydrothermal reaction, the total mass of the sample increased from 217 mg to
153 462 mg, with its color changed from black to brown.

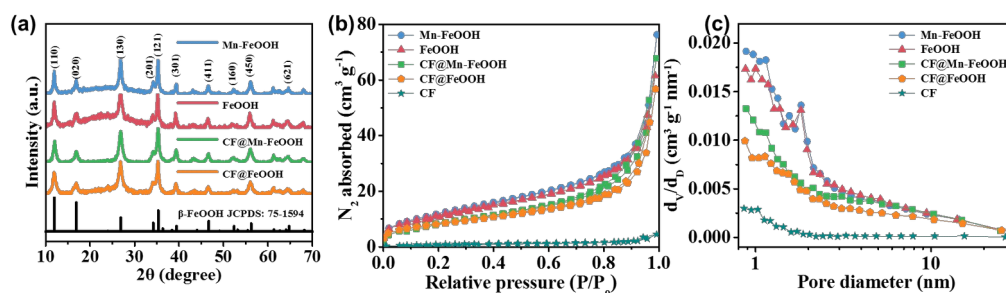
154

155 **3.1 Characterization of CF@Mn-FeOOH nanospindles**



157 **Figure 2.** SEM images of (a) & (b) oxidized carbon foam, (c) & (d) CF@FeOOH nanospindles, (e) &(f)
158 CF@Mn-FeOOH nanospindles. Energy dispersive spectroscopy (EDS) mapping images of CF@Mn-
159 FeOOH nanospindles are shown as (g) elements overlay, and (h) C K α 1, O K α 1, Fe K α 1, and Mn K α 1.

160 The SEM images in Figure 2 show the morphologies and microstructures of the obtained samples.
161 Figure 2(a) displays the inter-connected and integral frame of the carbon foam made of carbon fibers,
162 which is beneficial for the mass transfer of the ions in solution along the porous fibers. Figure 2(b)
163 shows the smooth surface of carbon fiber. Compared with Figures 2(b), Figures 2(c)-2(f) exhibit a rough
164 surface, indicating the loading of FeOOH and Mn-FeOOH nanospindles on the carbon fiber. It can be
165 seen in Figure 2(d) and 2(f) that the FeOOH and Mn-FeOOH nanospindles were homogeneously
166 distributed on the surface of carbon fiber, with the diameter of about 100 nm and length of 1 μ m. The
167 numerous evenly-distributed Mn-FeOOH nanospindles provided abundant active sites for arsenic
168 oxidation-adsorption. The EDS mapping images of the CF@Mn-FeOOH NSp shown in Figure 2(g) and
169 2(h) display the homogeneous distribution of C, O, Fe and Mn element through the backbone of CF,
170 suggesting that Mn-FeOOH nanospindles are evenly distributed on the carbon fiber, which further
171 promotes the high-efficient adsorption of arsenic.



172

173 **Figure 3.** (a) XRD patterns of CF@Mn-FeOOH, CF@FeOOH, Mn-FeOOH powder and FeOOH

174 powder; (b) BET and (c) BJH analyses of Mn-FeOOH powder, FeOOH powder, CF@Mn-FeOOH,

175 CF@FeOOH and melamine foam.

176 The crystal structure of the obtained samples was verified with XRD. Several typical peaks of

177 CF@FeOOH and CF@Mn-FeOOH at 11.94°, 16.92°, 26.9°, 34.22°, 35.33°, 46.69°, and 56.22° are

178 indexed to the planes of (110), (200), (130), (400), (211), (411), and (251) for β -FeOOH, respectively

179 (JCPDS No.75-1594) [39]. The four samples exhibit almost the same XRD pattern, suggesting that the

180 Mn doping would not change the crystal structure of FeOOH. However, when compare the unit cell

181 parameters of the four samples, a changing trade can be found that as Mn doping into the lattice of

182 FeOOH, the a and b axis would be compressed, while the c axis was stretched (Table S1, supporting

183 information). The XRD results demonstrate the single phase of Mn doped FeOOH and imply the

184 uniform distribution of Mn on FeOOH at atomic scale.

185 BET and BJH analyses were employed to analyze the specific surface area and pore characteristics of

186 the obtained samples as shown in Figure 3(b) and 3(c). The BET specific surface area of the samples

187 (Table S2, supporting information) illustrates that the specific surface areas were as followed: Mn-

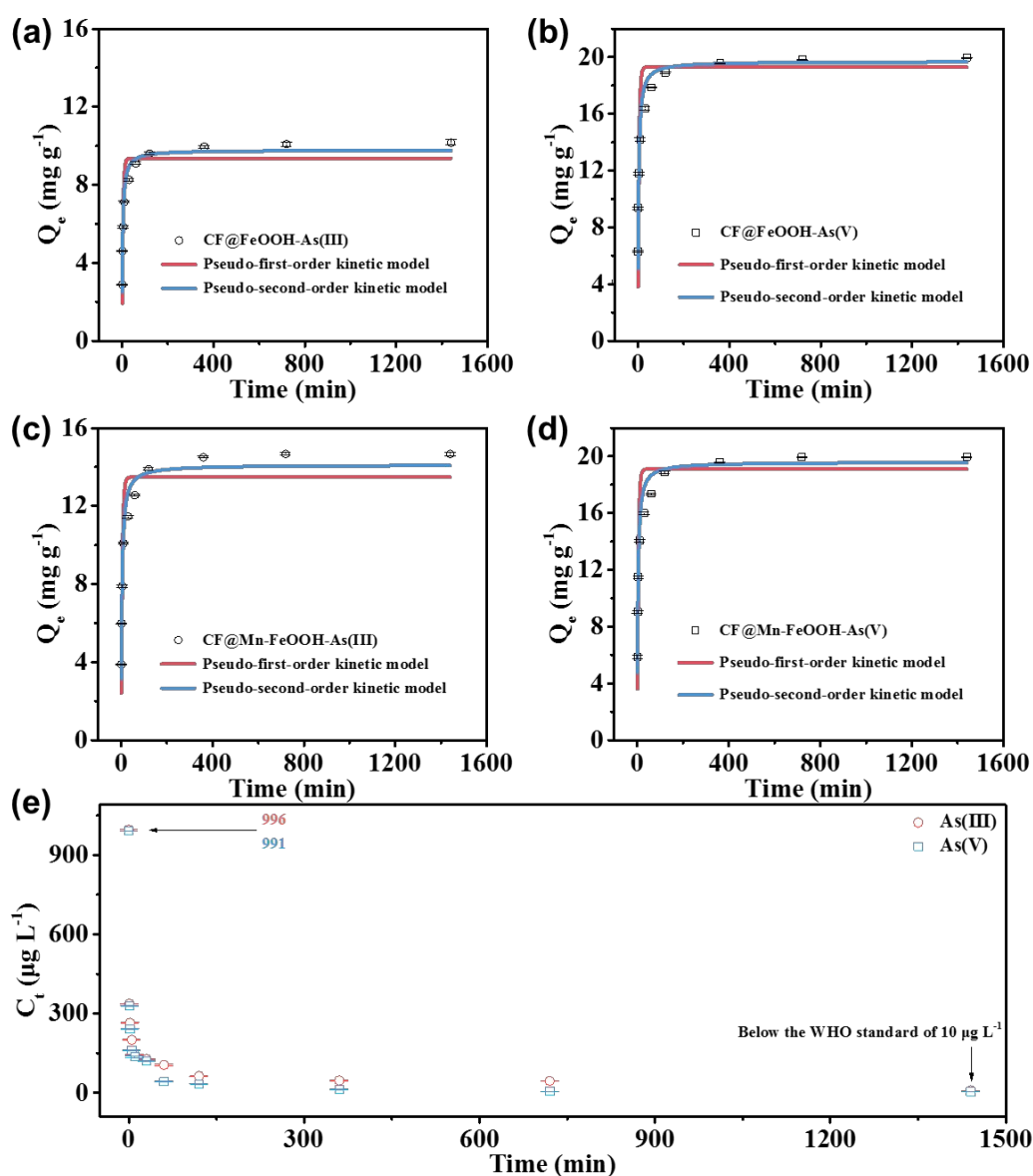
188 FeOOH ($45.10 \text{ m}^2 \text{ g}^{-1}$) > FeOOH ($42.68 \text{ m}^2 \text{ g}^{-1}$) > CF@Mn-FeOOH ($32.40 \text{ m}^2 \text{ g}^{-1}$) > CF@FeOOH (29.86

189 $\text{m}^2 \text{ g}^{-1}$) > CF ($3.67 \text{ m}^2 \text{ g}^{-1}$). It can be concluded that the specific surface area mainly originated from

190 FeOOH and Mn-FeOOH nanospindles. It can also be seen from BJH analyses that the micro/mesopores

191 were mainly derived from FeOOH and Mn-FeOOH nanospindles. Thus, the decoration of oxidized CF
 192 with FeOOH and Mn-FeOOH nanospindles further enlarged the specific surface area of CF@FeOOH
 193 and CF@Mn-FeOOH, by exposing more active sites for arsenic adsorption.

194 **3.2 Arsenic adsorption kinetics**



195
 196 **Figure 4.** (a-d) Adsorption kinetic model fittings of CF@FeOOH and CF@Mn-FeOOH adsorbing As
 197 in either 10 mg L⁻¹ of As(III) or As(V) solution, and (e) As removal kinetic by CF@Mn-FeOOH in 1
 198 mg L⁻¹ of As(III) or As(V) solution.

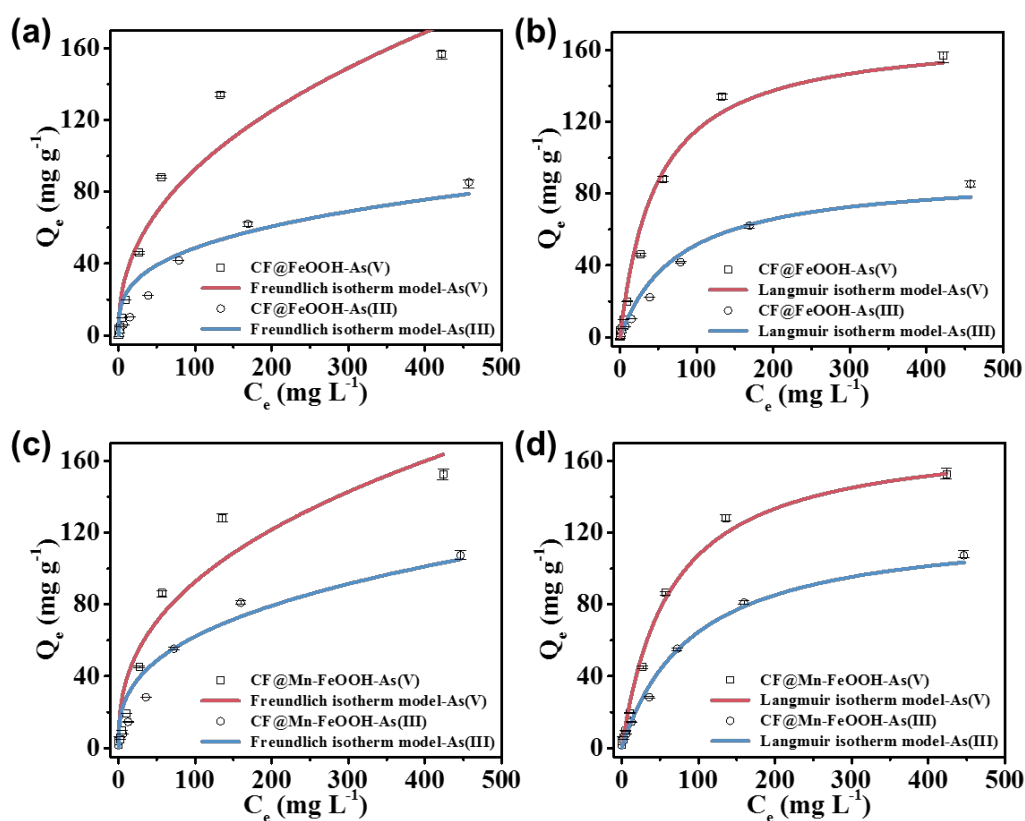
199 Figure 4(a-d) displays the time-dependent adsorption kinetic models fitting the adsorption behavior
200 of CF@FeOOH and CF@Mn-FeOOH in 10 mg L⁻¹ of arsenic solution. The specific fitting results are
201 displayed in Table S3 (supporting information) and the detailed information can be found in Text S1
202 (supporting information). After compare the two models of pseudo-first order kinetics model and
203 pseudo-second order kinetics model, it is manifest that the adjustment R² in the latter one are much
204 higher for both adsorbents, indicating the adsorption behavior towards As(III) and As(V) is more in line
205 with the pseudo-second-order kinetic model. This indicates the adsorptions of the two adsorbents were
206 of chemisorption nature [40]. As shown in Figure 4, for As(V) adsorption, each of the two adsorbents
207 reached more than 87% of its maximal possible As(V) content within 60 minutes. Further, the treated
208 solution meets the demand for drinking of WHO-MCL (<10 µg L⁻¹) within 24 h, indicating that the two
209 adsorbents possess excellent adsorption ability towards As(V) (Figure S2, supporting information).

210 For As(III) adsorption, CF@FeOOH could reach 50% of its maximal adsorption capacity within 60
211 min, while CF@Mn-FeOOH showed a higher maximal adsorbing capacity as 72%. This can be
212 ascribed to the fact that Mn(IV) could oxidize As(III) to As(V), which is more easily to adsorb by
213 Fe(III). Under the experimental conditions, FeOOH dissociated into Fe³⁺ or FeO⁺, and combined with
214 As(III) to As(V) to form Fe-O-As chemical bond [13, 26]. In pH-neutral solution, As(V) ion cluster is
215 larger than that of As(III) and exhibits electronegativity, resulting in well combination with Fe³⁺ or
216 FeO⁺. However, the bond formed between As(III) and Fe³⁺ or FeO⁺ was much weaker than that of
217 As(V), hindering the forming of a stable chemical bond, which then led to lower adsorption capacity
218 [41]. The adsorption kinetic data indicate that FeOOH is more effective in adsorbing As(V) in aqueous
219 solution than As(III), therefore doping Mn can increase its adsorption capacity towards As(III).

220 In order to verify the potential application of the adsorbent, a simulated high arsenic groundwater

221 solution of arsenate and arsenite at 1 mg L^{-1} were used respectively. The process of As removal by
 222 CF@Mn-FeOOH was illustrated in Figure 5(e). It is noticeable that the residual arsenic concentration
 223 was reduced sharply (around 70% decrease) in the first minute both for As(III) and As(V) solution.
 224 Furthermore, after adsorbing for 24 h, the total As concentration for As(III) and As(V) solution turned
 225 out to be 9.4 and $4.4 \text{ } \mu\text{g L}^{-1}$, respectively, both lower than the WHO-MCL for drinkable water. These
 226 results make the adsorbent more attractive in practice.

227 3.3 Arsenic adsorption isotherms



228
 229 **Figure 5.** Adsorption isotherm models fitting of (a) and (b) CF@FeOOH, and (c) and (d) CF@Mn-
 230 FeOOH, for adsorbing As(V) and As(III).

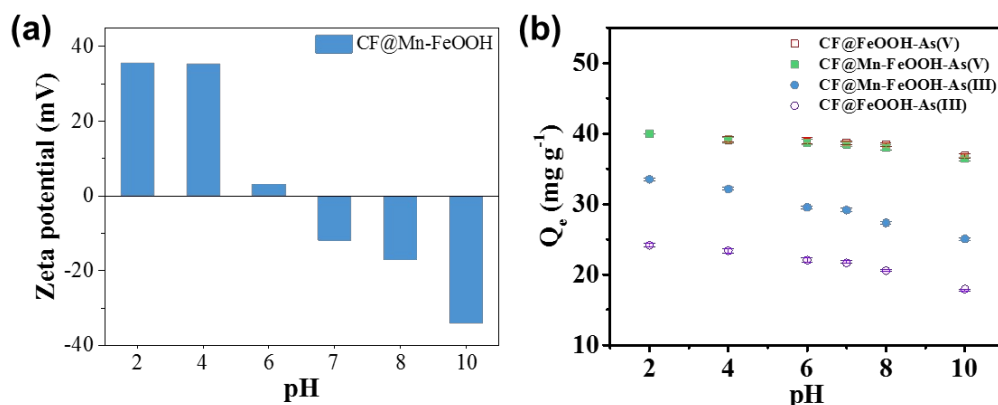
231 Arsenic adsorption isotherms of CF@FeOOH and CF@Mn-FeOOH for adsorbing As(V) and As(III)
 232 were examined and the corresponding results were illustrated in Figure 5. All the isotherms were fitted

233 with both Langmuir and Freundlich isotherm models, with detailed information shown in Text S2. The
234 detailed parameters for the fitting results are displayed in Table S4 (supporting information), which
235 reveal that both adsorbents obey a Langmuir isotherm model. Therefore, the adsorbing of arsenic was a
236 single-layer adsorption process, indicating that the adsorption sites were homogeneously dispersed at
237 the outer layer of the adsorbents [13].

238 In order to investigate the maximum adsorption capacity at equilibrium, the dosages of the
239 adsorbents were fixed at 0.5 g L⁻¹ even in solution of high arsenic concentration, hence the active sites
240 of the adsorbents can be substantially occupied. It turned out that the maximal adsorption capacity for
241 As(III) and As(V) by CF@Mn-FeOOH under 500 mg L⁻¹ arsenic concentration were 107.3 and 152.5
242 mg g⁻¹, respectively, while for CF@FeOOH the data were 85.4 and 156.7 mg g⁻¹. It is manifest that
243 CF@Mn-FeOOH had superior adsorption capacity towards As(III) than CF@FeOOH, but similar
244 adsorption capability to As(V), which are in consistent of the results in adsorption kinetics study (3.2).
245 This excellent adsorption capability towards As(III) and As(V) surpasses many other reported
246 adsorbents [23, 28-30, 42], which mainly benefited from the 3D interconnected network in CF@Mn-
247 FeOOH contributing to the rapid ion transportation in aqueous solution, the homogeneous distribution
248 of oxidative Mn(IV) helping to transform As(III) to As(V), as well as the ample active sites on the Mn-
249 FeOOH nanospindles [26].

250 **3.4 Effect of pH on arsenic adsorption**

251



252

253 **Figure 6.** (a) Zeta potential of CF@Mn-FeOOH under different pH, and (b) Influence of initial pH on

254 the adsorption capacity of As(III) and As(V) by CF@FeOOH and CF@Mn-FeOOH.

255 Initial pH of the solution may be one of the most important parameters that affects adsorption

256 capacity of adsorbents. Hence, the zeta potential of CF@Mn-FeOOH under different pH and the

257 influence of pH (from 2 to 10) on the removal of As(V) and As(III) by CF@FeOOH and CF@Mn-

258 FeOOH was studied and the results were presented in Figure 6. It can be seen that the zeta potential of

259 the CF@Mn-FeOOH decreased as the pH value increased from 2 to 10 (Figure 6(a)). Both adsorbents

260 showed a larger adsorption capacity for both As(V) and As(III) at a lower pH, and the adsorption

261 capacity declined as the pH increased (Figure 6(b)). Meanwhile, the adsorption capacity for As(V) was

262 higher than that for As(III) for a given adsorbent. The reason is that when the pH was low (<7), the

263 hydroxyl groups on the surface of the adsorbents were protonated. Thus, the adsorbents surfaces were

264 positively charged under acidic conditions, while under increasingly alkaline conditions, the adsorbents

265 surfaces were negatively charged. Based on the Eh-pH diagram of arsenic [43], As(III) is stable in the

266 form of H₃AsO₃ with pH from 4 to 9, while H₂AsO₃⁻ is the stable form for pH >9. As for As(V),

267 H₂AsO₄⁻ is the predominant species for pH from 2 to 7, while HAsO₄²⁻ is the predominant form for

268 pH >7. In aqueous solution with the pH <7, the positively charged adsorbents would uptake more of the

269 anion H_2AsO_4^- (As(V)) through electrostatic attraction, while adsorb less nonionic H_3AsO_3 (As(III)).
270 This explains why for the same kind of adsorbent, the adsorbed amount of As(V) was higher than that
271 of As(III). When the pH value increased, the adsorbents would coordinate with OH^- , and their
272 negatively charged surface would repulse the arsenic anions, resulting in a lower adsorption capacity.
273 This is consistent with our experiment results that the adsorption capacity towards arsenic decreases
274 with the pH value increases for the same kind of adsorbent.

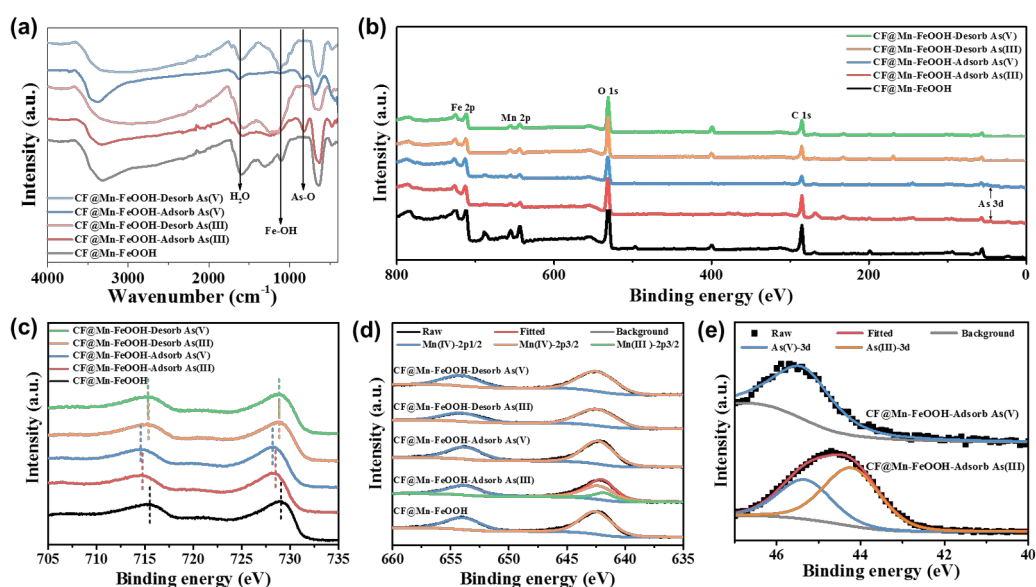
275 When adsorbing As(V), CF@Mn-FeOOH and CF@FeOOH revealed little difference in adsorption
276 capacity as shown in Figure 6, with CF@FeOOH slightly larger than that of CF@Mn-FeOOH. This
277 may be due to the fact that Mn atoms blocked some of the active sites of FeOOH in CF@Mn-FeOOH,
278 thus adsorbed less As(V) than CF@FeOOH [24]. Another reason might be that the doped Mn
279 decreased the mass of FeOOH and therefore decreased the adsorption ability of a unit mass of
280 adsorbent. On the contrary, when adsorbing As(III), Mn(IV) played the irreplaceable role of oxidizing
281 the hard-to-adsorbed As(III) to the easily adsorbed As(V), which was subsequently adsorbed by
282 FeOOH. In the process of adsorbing As(III), Mn(IV) cooperated with FeOOH and behaved much better
283 than CF@FeOOH.

284 **3.5 Effect of co-existing competing anions towards arsenic adsorption**

285 The influences of four common co-existing competing anions (Cl^- , HCO_3^- , SO_4^{2-} and PO_4^{3-}) in high
286 arsenic groundwater [44] on the removal of As(V) and As(III) by CF@FeOOH and CF@Mn-FeOOH
287 were investigated. Two different concentrations for each kind of ions (0.1 and 1 mmol L^{-1}) were
288 conducted in the experiment. It is indicated in the results shown in Figure S3 (supporting information),
289 the influence of Cl^- and HCO_3^- (0.1 and 1 mmol L^{-1}) on the adsorption capacity of both As(III) and
290 As(V) by the two adsorbents is almost unchanged. Similar negligible effect was observed for lower

291 concentration of SO_4^{2-} (0.1 mmol L^{-1}). However, at higher concentration, SO_4^{2-} (1 mmol L^{-1}) depressed the
 292 adsorption of As(III) and As(V), especially for As(III). PO_4^{3-} manifested the greatest impact on the two
 293 adsorbents. The adsorption capacity of both adsorbents reduced drastically when PO_4^{3-} co-exist with
 294 arsenic in solution. A possible reason is that both SO_4^{2-} and PO_4^{3-} carry more charges, which cause them
 295 easily to coordinate with FeOOH [26]. This results in the competition between the arsenic anions and
 296 the co-existing anions for the adsorption sites on FeOOH, thereby affecting the adsorption capacity of
 297 both adsorbents. Cl^- and HCO_3^- are smaller anions when compared to SO_4^{2-} and PO_4^{3-} , this render to their
 298 weak ability to compete with arsenic for sites on FeOOH. Hence, the effect of Cl^- and HCO_3^- towards the
 299 adsorption of arsenic by the two adsorbents was almost negligible.

300 3.6 Oxidation-adsorption mechanism of CF@Mn-FeOOH



301
 302 **Figure 7.** (a) FTIR analyses of original CF@Mn-FeOOH and CF@Mn-FeOOH after
 303 adsorbing/desorbing As(III)/As(V). XPS analyses: (a) full spectra, (b) Fe 2p, (c) Mn 2p of original
 304 CF@Mn-FeOOH and CF@Mn-FeOOH after adsorbing/desorbing As(III)/As(V). (d) As 3d spectra of
 305 CF@Mn-FeOOH adsorbing As(III)/As(V).

306 According to the above results on arsenic removal by CF@Mn-FeOOH and CF@FeOOH with
307 different experiment parameters including reaction time, initial concentration and solution pH,
308 CF@Mn-FeOOH delivered better adsorption capacity towards As(V) and As(III). In order to verify the
309 synergistic effect of Mn(IV) and FeOOH (where Mn(IV) oxidized As(III) to As(V), while FeOOH
310 adsorbed both of As(III) and As(V)), FTIR and XPS analyses were utilized.

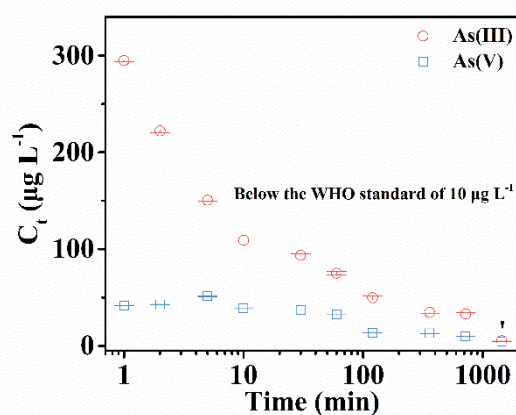
311 The FTIR analyses were utilized to verify the chemical reaction process between the adsorbent and
312 adsorbate (Figure 7(a)). The peak at around 1620 cm^{-1} was attributed to the deformation of water
313 molecules, indicating there existed physisorbed water on the samples [45]. For the original CF@Mn-
314 FeOOH spectrum, the peak around 1120 cm^{-1} can be assigned to the bending vibration of the hydroxyl
315 group (Fe-OH) [46]. After adsorbing As(III), the peak of Fe-OH disappeared while a new peak that
316 corresponded to the As-O stretching vibration appeared at around 820 cm^{-1} [46]. This indicated that
317 As(III) was adsorbed onto CF@Mn-FeOOH and formed the Fe-O-As chemical bond, thus the Fe-OH
318 disappeared while As-O appeared. It was also suggested that As was bound as a surface complex rather
319 than a precipitated solid phase. The similar phenomena could also be seen in the spectra of CF@Mn-
320 FeOOH adsorbing and desorbing As(V), where the peak of Fe-OH disappeared while As-O emerged,
321 respectively.

322 Figure 7(b-e) displayed the XPS data of full spectra, Fe 2p spectra, Mn 2p spectra, and As 3d spectra
323 for the original CF@Mn-FeOOH and the samples after adsorbing/desorbing As(III)/As(V). In Figure
324 7b, the five samples exhibited the same symbolic peaks of C 1s, O 1s, Fe 2p and Mn 2p, with the
325 samples adsorbing As(III)/As(V) showed additional As 3p peaks, in accordance with the adsorption
326 process of arsenic. CF@Mn-FeOOH in Figure 7(c) exhibited peaks at 711.1 and 724.8 eV,
327 corresponding to Fe 2p_{3/2} and Fe 2p_{1/2}, respectively. After the adsorption of As(III), the peaks shifted

328 to higher energy of Fe 2p_{3/2} and Fe 2p_{1/2}, locating at 711.6 and 725.4 eV, respectively. This may be
329 attributed to the formation of Fe-O-As bonds in the arsenic adsorption process, during which the iron
330 and arsenic chemically interact with each other [13, 26]. An even more positive shift can be observed
331 after the adsorption of As(V), with peaks located at 711.7 and 725.5 eV corresponding to Fe 2p_{3/2} and
332 Fe 2p_{1/2}, respectively. The results indicate that the affinity between CF@Mn-FeOOH and As(V) was
333 stronger than that of As(III), in line with the fact that the adsorption capacity towards As(V) was higher
334 than that of As(III). After the desorbing of As(III) and As(V), the peaks of Fe 2p_{3/2} and Fe 2p_{1/2} for
335 both samples resumed to almost the same as that of original CF@Mn-FeOOH, demonstrating the
336 dissociation of the Fe-O-As chemical bond.

337 The Mn 2p spectra of the three samples are shown in Figure 7(d). The Mn 2p spectrum of the
338 original CF@Mn-FeOOH can be deconvoluted into Mn(IV)-2p_{1/2} and Mn(IV)-2p_{3/2}, situated at 654.1
339 and 642.4 eV, respectively. The Mn 2p spectrum of CF@Mn-FeOOH after adsorbing As(V) displays
340 almost the same curve as that of original CF@Mn-FeOOH, demonstrating that there was no valence
341 change of Mn during the adsorption process. For the Mn 2p spectrum of CF@Mn-FeOOH after
342 adsorbing As(III), however, not only did the peak intensity decrease, but also the spectrum could be
343 deconvoluted into three peaks, i.e. 641.7, 642.4, and 654.1 eV for Mn(III)2p_{3/2}, Mn(IV) 2p_{3/2}, and
344 Mn(IV) 2p_{1/2}, respectively. It suggests that there was chemical reaction between Mn(IV) and As(III),
345 probably Mn(IV) oxidized As(III) into As(V) and generated Mn(III), which is in consistent with the
346 result that there are smaller contributions to the spectrum from Mn(IV), and that peaks of Mn(III)
347 appears in the Mn 2p spectrum. The Mn 2p spectra of the samples after desorbing As(III) and As(V)
348 were almost the same as that of original CF@Mn-FeOOH, indicating that Mn(III) was oxidized to
349 Mn(IV) in the process of regeneration.

350 The As 3d spectra of CF@Mn-FeOOH after adsorbing As(III) and As(V) further proved the
 351 functionality of Mn(IV) oxidation (Figure 7(e)). After adsorbing As(V), the As 3d spectrum of
 352 CF@Mn-FeOOH can only be deconvoluted into one peak locating at 45.4 eV that corresponded to
 353 As(V). Differently, after adsorbing As(III), the As 3d spectrum of CF@Mn-FeOOH can be
 354 deconvoluted into two peaks, i.e. 45.4 and 44.2 eV, attributing to As(V) and As(III), respectively [46,
 355 47]. It was manifest that the doped Mn(IV) within the CF@Mn-FeOOH could oxidize As(III) to more
 356 easily adsorbed As(V).



357

358 **Figure 8.** The residual arsenic concentration separated to As(III) and As(V) species in As(III) solution
 359 when using CF@Mn-FeOOH to adsorb.

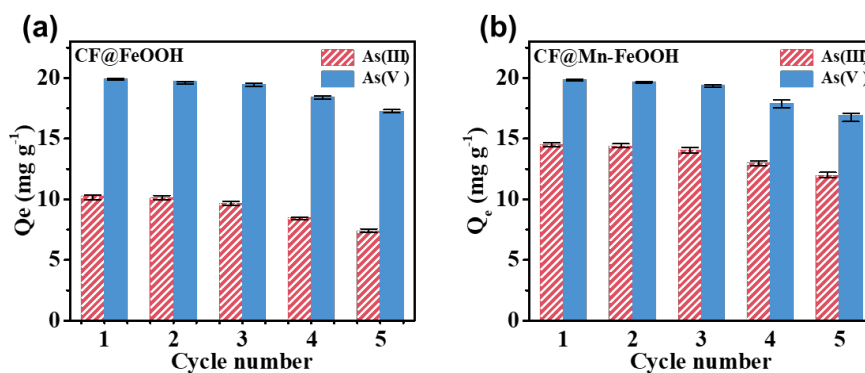
360 To further prove the oxidization of As(III) to As(V) during adsorbing process, and then explore the
 361 “oxidation-adsorption” behavior of CF@Mn-FeOOH towards As(III), As speciation was analyzed using
 362 AFS during arsenic removal by CF@Mn-FeOOH in 1 mg L⁻¹ of arsenite solution, as shown in Figure 8.
 363 It can be seen that the As(III) concentration reduced from 996 to 109 µg L⁻¹ in the first 10 minutes, then
 364 slowly decreased to around 5 µg L⁻¹ in the later adsorption stage (24 h). As(V) appeared at the very
 365 beginning of the process and peaked at 51 µg L⁻¹ at the 5th minute and then gradually decreased to
 366 around 4.5 µg L⁻¹. It is suggested that As(III) started to transform to As(V) at the beginning, especially

367 strongly within the first 5 minutes, proving the above conclusion. This can be ascribed to the numerous
368 vacant active adsorption sites [48] of CF@Mn-FeOOH in the first 10 minutes of the adsorbing process.
369 Mn(IV) doped on the FeOOH nanospindles simultaneously oxidized the adsorbed As(III) to As(V),
370 which was then *in-situ* adsorbed by FeOOH nanospindles, which is consistent in the XPS results above.
371 At the same time, Mn(IV) also oxidized As(III) in the solution to As(V) [24]. FeOOH nanospindles
372 kept adsorbing As(III) and oxidized As(V) from the solution as well as the *in-situ* oxidized As(V)
373 transformed from As(III) on the nanospindles, resulting in less active adsorption sites and inferior
374 adsorbing ability in the later stage. Therefore, As(III) and As(V) concentration in the residual solution
375 decreased slower after the first 10 minutes.

376 With the novel material described here, the introduction of Mn(IV) compensated for this deficiency
377 by oxidizing As(III) into As(V). The synergistic effect of “oxidation (Mn(IV))-adsorption (FeOOH)” on
378 the surfaces of CF@Mn-FeOOH results in the excellent adsorption capability towards both As(III) and
379 As(V), showing much superior adsorption capacity when compared with CF@FeOOH.

380 **3.7 Desorption and reusability study**

381 In addition to the high adsorption capacity, when considering the practical application and realistic
382 cost, it is also important for adsorbents to maintain their high ability to rapidly adsorb arsenic even after
383 recycling for many times. The reusability of the two adsorbents is displayed in Figure 9.



384

385 **Figure 9.** Reusability of (a) CF@FeOOH and (b) CF@Mn-FeOOH towards the adsorption of As(III)
 386 and As(V).

387 As seen from Figure 9, the two adsorbents maintained a high value of maximum adsorption density
 388 (mg/g) of As(V) even after the first four regenerations. At the fifth cycle, the maximal adsorption
 389 density of CF@FeOOH and CF@Mn-FeOOH for As(V) were 17.3 and 16.9 mg g^{-1} , maintaining 86%
 390 and 85% of their initial maximum adsorption density.

391 Compared to As(V), the two adsorbents showed relatively smaller but more stable adsorption
 392 capacity towards As(III). CF@Mn-FeOOH (14.5 mg g^{-1}) was able to adsorb 41.7% more As(III) than
 393 CF@FeOOH (10.2 mg g^{-1}) in their initial adsorption. After five cycles, the maximal adsorption density
 394 of CF@Mn-FeOOH towards As(III) remained 82% of its initial value, while CF@FeOOH remained
 395 72% of its initial value. Both adsorbents exhibited excellent reusability towards the adsorption of As(V)
 396 and As(III). The XRD results can also prove the superior stability and reusability of the adsorbents.
 397 After the 1st and 5th adsorbing/desorbing the As(III)/As(V), the XRD patterns of the CF@FeOOH and
 398 CF@Mn-FeOOH remained almost the same as their original samples (Figure S4, supporting
 399 information).

400 Table S5 (supporting information) shows the comparison of adsorption capacity between our
 401 prepared CF@Mn-FeOOH and various other adsorbents. The performance of CF@Mn-FeOOH towards

402 the adsorbing of As(III) and As(V) is seen to be superior to most of the reported adsorbents. Moreover,
403 with low cost, CF@Mn-FeOOH is easy to prepare and to reuse, thus showing high potential for treating
404 high arsenic contaminated water.

405 **Conclusions**

406 Arsenic pollution in groundwater has become a serious environmental issue, which demands
407 advanced effective adsorbents for high-efficient arsenic removal. Herein, a free-standing composite of
408 Mn doped β -FeOOH nanospindles decorated carbonized melamine foam (CF@Mn-FeOOH) has been
409 prepared through a facile hydrothermal method, which displayed a "oxidation (Mn(IV))-adsorption
410 (Fe(III))" bifunctionality and the characteristic of free standing. The composite is able to adsorb arsenic
411 (both As(III) and As(V)) efficiently and can be easily reused. The oxidation and adsorption
412 characteristics of CF@Mn-FeOOH regarding As(III), and As(V) have been systematically investigated.
413 The maximal adsorption capacities for As(III) and As(V) were turned out to be 107 and 152 mg g⁻¹,
414 respectively, under initial arsenic concentration of 500 mg L⁻¹ at pH=7. Meanwhile the simulated high
415 arsenic groundwater can be treated to meet WHO-MCL for As within 24 h. The kinetic adsorption
416 behavior of CF@Mn-FeOOH fitted well with the pseudo-second-order kinetic equation, suggesting the
417 adsorbing of arsenic was mainly through chemical bonding; while the isotherm adsorption behavior was
418 more consistent with the Langmuir isotherm model, demonstrating a monolayer adsorbing behavior.
419 The adsorption capacity of CF@Mn-FeOOH towards arsenic decreased with the pH value. For
420 reusability, this adsorbent was proved to maintain more than 80.0% of its initial removal capability
421 (As(III): 82%, As(V): 85%, respectively) after five adsorption/desorption cycles, showing a good
422 recycling stability. In summary, CF@Mn-FeOOH is a highly efficient adsorbent to remove arsenic (both
423 As(III) and As(V)) from arsenic contaminated water and is a promising material for practical

424 applications.

425

426 **Author information**

427 **Corresponding authors**

428 Bing Yan - School of Environmental Studies, China University of Geosciences, Wuhan 430074,

429 PR China; Department of Civil and Environmental Engineering, University of California, Berkeley, CA

430 94720-1710, USA. Email: yanbing@cug.edu.cn

431 Ashok J. Gadgil - Department of Civil and Environmental Engineering, University of California,

432 Berkeley, CA 94720-1710, USA. Email: ajgadgil@berkeley.edu

433

434 **Co-authors**

435 Tian Liang – Faculty of materials science and chemistry, China University of Geosciences, Wuhan

436 430074, PR China.

437 Xiaohui Yang - Faculty of materials science and chemistry, China University of Geosciences,

438 Wuhan 430074, PR China.

439

440 **CREDIT author contribution statement**

441 Bing Yan and Ashok J. Gadgil conceived and designed the experiments. Tian Liang and Xiaohui

442 Yang synthesized and characterized the materials. Bing Yan and Ashok J. Gadgil analyzed the results

443 and wrote and revised the manuscript. The manuscript was written through the contributions of all

444 authors.

445

446 **Declaration of Competing Interest**

447 The authors declare no competing financial interest.

448

449 **Acknowledgements**

450 Bing Yan gratefully acknowledges the financial support of the National Natural Science
451 Foundation of China (NSFC) Grants NO. 41807201. We also thank the support of China Scholarship
452 Council (CSC) Grant NO. 201906415011 (Bing Yan) and NO. 201906410068 (Tian Liang).

453

454 **References**

- 455 [1] S. Muthu Prabhu, C.M. Park, A. Shahzad, D.S. Lee, Designed synthesis of sulfide-rich bimetallic-
456 assembled graphene oxide sheets as flexible materials and self-tuning adsorption cum oxidation
457 mechanisms of arsenic from water, *J. Mater. Chem. A*, 7 (2019) 12253-12265.
- 458 [2] A. Jain, V.K. Sharma, O.S. Mbuya, Removal of arsenite by Fe(VI), Fe(VI)/Fe(III), and
459 Fe(VI)/Al(III) salts: effect of pH and anions, *J. Hazard. Mater.*, 169 (2009) 339-344.
- 460 [3] L. Rodriguez-Lado, G. Sun, M. Berg, Q. Zhang, H. Xue, Q. Zheng, C.A. Johnson, Groundwater
461 arsenic contamination throughout China, *Science*, 341 (2013) 866-868.
- 462 [4] M. Habuda-Stanic, M. Nujic, Arsenic removal by nanoparticles: a review, *Environ. Sci. Pollut. Res.*
463 *Int.*, 22 (2015) 8094-8123.
- 464 [5] M. Egal, C. Casiot, G. Morin, M. Parmentier, O. Bruneel, S. Lebrun, F. Elbaz-Poulichet, Kinetic
465 control on the formation of tooeleite, schwertmannite and jarosite by *Acidithiobacillus ferrooxidans*
466 strains in an As(III)-rich acid mine water, *Chem. Geol.*, 265 (2009) 432-441.
- 467 [6] S.H. Ahoranta, M.E. Kokko, S. Papirio, B. Ozkaya, J.A. Puhakka, Arsenic removal from acidic
468 solutions with biogenic ferric precipitates, *J. Hazard. Mater.*, 306 (2016) 124-132.
- 469 [7] L. Yan, S. Hu, C. Jing, Recent progress of arsenic adsorption on TiO₂ in the presence of coexisting
470 ions: A review, *J. Environ. Sci-China*, 49 (2016) 74-85.
- 471 [8] Y. Matsui, N. Shirasaki, T. Yamaguchi, K. Kondo, K. Machida, T. Fukuura, T. Matsushita,
472 Characteristics and components of poly-aluminum chloride coagulants that enhance arsenate removal
473 by coagulation: Detailed analysis of aluminum species, *Water Res.*, 118 (2017) 177-186.
- 474 [9] H. Tian, G. Zhuang, A. Ma, C. Jing, Arsenic interception by cell wall of bacteria observed with
475 surface-enhanced Raman scattering, *J. Microbiol. Meth.*, 89 (2012) 153-158.
- 476 [10] S. Lin, H. Yang, Z. Na, K. Lin, A novel biodegradable arsenic adsorbent by immobilization of iron
477 oxyhydroxide (FeOOH) on the root powder of long-root *Eichhornia crassipes*, *Chemosphere*, 192
478 (2018) 258-266.
- 479 [11] A. Ortega, I. Oliva, K.E. Contreras, I. González, M.R. Cruz-Díaz, E.P. Rivero, Arsenic removal
480 from water by hybrid electro-regenerated anion exchange resin/electrodialysis process, *Sep. Purif.*
481 *Technol.*, 184 (2017) 319-326.
- 482 [12] W. Wong, H.Y. Wong, A.B. Badruzzaman, H.H. Goh, M. Zaman, Recent advances in exploitation
483 of nanomaterial for arsenic removal from water: a review, *Nanotechnology*, 28 (2017) 042001.
- 484 [13] D. Fu, Z. He, S. Su, B. Xu, Y. Liu, Y. Zhao, Fabrication of alpha-FeOOH decorated graphene

485 oxide-carbon nanotubes aerogel and its application in adsorption of arsenic species, *J. Colloid Interf.*
486 *Sci.*, 505 (2017) 105-114.

487 [14] F. Peng, T. Luo, L. Qiu, Y. Yuan, An easy method to synthesize graphene oxide-FeOOH
488 composites and their potential application in water purification, *Mater. Res. Bull.*, 48 (2013) 2180-2185.

489 [15] J.S. Zhang, R.S. Stanforth, S.O. Pehkonen, Effect of replacing a hydroxyl group with a methyl
490 group on arsenic (V) species adsorption on goethite (α -FeOOH), *J. Colloid Interf. Sci.*, 306 (2007)
491 16-21.

492 [16] L. Feng, M. Cao, X. Ma, Y. Zhu, C. Hu, Superparamagnetic high-surface-area Fe₃O₄ nanoparticles
493 as adsorbents for arsenic removal, *J. Hazard. Mater.*, 217-218 (2012) 439-446.

494 [17] C. Shan, M. Tong, Efficient removal of trace arsenite through oxidation and adsorption by
495 magnetic nanoparticles modified with Fe-Mn binary oxide, *Water Res.*, 47 (2013) 3411-3421.

496 [18] H.L. Lien, R.T. Wilkin, High-level arsenite removal from groundwater by zero-valent iron,
497 *Chemosphere*, 59 (2005) 377-386.

498 [19] T.J. Sorg, A.S. Chen, L. Wang, Arsenic species in drinking water wells in the USA with high
499 arsenic concentrations, *Water Res.*, 48 (2014) 156-169.

500 [20] A. Vogelin, S.J. Hug, Catalyzed Oxidation of Arsenic(III) by Hydrogen Peroxide on the Surface
501 of Ferrihydrite: An in Situ ATR-FTIR Study, *Environ. Sci. Technol.*, 37 (2003) 972-978.

502 [21] C.M. McCann, C.L. Peacock, K.A. Hudson-Edwards, T. Shrimpton, N.D. Gray, K.L. Johnson, In
503 situ arsenic oxidation and sorption by a Fe-Mn binary oxide waste in soil, *J. Hazard. Mater.*, 342 (2018)
504 724-731.

505 [22] G. Zhang, H. Liu, J. Qu, W. Jefferson, Arsenate uptake and arsenite simultaneous sorption and
506 oxidation by Fe-Mn binary oxides: influence of Mn/Fe ratio, pH, Ca²⁺, and humic acid, *J. Colloid*
507 *Interf. Sci.*, 366 (2012) 141-146.

508 [23] G. Zhang, J. Qu, H. Liu, R. Liu, R. Wu, Preparation and evaluation of a novel Fe-Mn binary oxide
509 adsorbent for effective arsenite removal, *Water Res.*, 41 (2007) 1921-1928.

510 [24] S. Tresintsi, K. Simeonidis, S. Estrade, C. Martinez-Boubeta, G. Vourlias, F. Pinakidou, M.
511 Katsikini, E.C. Paloura, G. Stavropoulos, M. Mitrakas, Tetravalent manganese ferrihydrite: a novel
512 nano-adsorbent equally selective for As(III) and As(V) removal from drinking water, *Environ. Sci.*
513 *Technol.*, 47 (2013) 9699-9705.

514 [25] F. Pinakidou, M. Katsikini, E.C. Paloura, K. Simeonidis, E. Mitraka, M. Mitrakas, Monitoring the
515 role of Mn and Fe in the As-removal efficiency of tetravalent manganese ferrihydrite nanoparticles from
516 drinking water: An X-ray absorption spectroscopy study, *J. Colloid Interf. Sci.*, 477 (2016) 148-155.

517 [26] X. Ge, Y. Ma, X. Song, G. Wang, H. Zhang, Y. Zhang, H. Zhao, beta-FeOOH Nanorods/Carbon
518 Foam-Based Hierarchically Porous Monolith for Highly Effective Arsenic Removal, *ACS Appl. Mater.*
519 *Interf.*, 9 (2017) 13480-13490.

520 [27] F. Chang, J. Qu, H. Liu, R. Liu, X. Zhao, Fe-Mn binary oxide incorporated into diatomite as an
521 adsorbent for arsenite removal: preparation and evaluation, *J. Colloid Interf. Sci.*, 338 (2009) 353-358.

522 [28] B. Chen, Z. Zhu, Y. Guo, Y. Qiu, J. Zhao, Facile synthesis of mesoporous Ce-Fe bimetal oxide and
523 its enhanced adsorption of arsenate from aqueous solutions, *J. Colloid Interf. Sci.*, 398 (2013) 142-151.

524 [29] K. Gupta, U.C. Ghosh, Arsenic removal using hydrous nanostructure iron(III)-titanium(IV) binary
525 mixed oxide from aqueous solution, *J. Hazard. Mater.*, 161 (2009) 884-892.

526 [30] S. Shevade, R.G. Ford, Use of synthetic zeolites for arsenate removal from pollutant water, *Water*
527 *Res.*, 38 (2004) 3197-3204.

528 [31] Z. Wu, W. Li, P.A. Webley, D. Zhao, General and controllable synthesis of novel mesoporous

529 magnetic iron oxide@carbon encapsulates for efficient arsenic removal, *Adv. Mater.*, 24 (2012) 485-
530 491.

531 [32] G. Zhang, Z. Ren, X. Zhang, J. Chen, Nanostructured iron(III)-copper(II) binary oxide: a novel
532 adsorbent for enhanced arsenic removal from aqueous solutions, *Water Res.*, 47 (2013) 4022-4031.

533 [33] I. Andjelkovic, D.N.H. Tran, S. Kabiri, S. Azari, M. Markovic, D. Losic, Graphene Aerogels
534 Decorated with α -FeOOH Nanoparticles for Efficient Adsorption of Arsenic from Contaminated
535 Waters, *ACS Appl. Mater. Interf.*, 7 (2015) 9758-9766.

536 [34] W.W. Meng X.G, Speciation of arsenic by disposable cartridges, Book of posters of the third
537 international conference on arsenic exposure and health effects, (1998).

538 [35] H. Guo, S. Yang, X. Tang, Y. Li, Z. Shen, Groundwater geochemistry and its implications for
539 arsenic mobilization in shallow aquifers of the Hetao Basin, Inner Mongolia, *The Science of the total*
540 *environment*, 393 (2008) 131-144.

541 [36] Xiu-Ping Yan, Xue-Bo Yin, Xi-Wen He, Y. Jiang., Flow Injection On-Line Sorption
542 Preconcentration Coupled with Hydride Generation Atomic Fluorescence Spectrometry for
543 Determination of (Ultra)trace Amounts of Arsenic(III) and Arsenic(V) in Natural Water Samples, *Anal.*
544 *Chem.*, 74 (2002) 2162-2166.

545 [37] S. Music , G.P. Santana, G. Smit, V.K. Gargd., Fe Mossbauer, FT-IR and TEM investigations of
546 Fe-oxide powders obtained from concentrated FeCl solutions, *Journal of Alloys and Compounds*, 278
547 (1998) 291-301.

548 [38] N. Nishida, S. Amagasa, H. Ito, Y. Kobayashi, Y. Yamada, Manganese-doped ferrihydrite nano-
549 urchins produced by chemical methods, *Hyperfine Interactions*, 239 (2018).

550 [39] Y. Piao, J. Kim, H.B. Na, D. Kim, J.S. Baek, M.K. Ko, J.H. Lee, M. Shokouhimehr, T. Hyeon,
551 Wrap-bake-peel process for nanostructural transformation from beta-FeOOH nanorods to biocompatible
552 iron oxide nanocapsules, *Nat. Mater.*, 7 (2008) 242-247.

553 [40] H.-J. Hong, J.-S. Yang, B.-K. Kim, J.-W. Yang, Arsenic Removal Behavior by Fe-Al Binary Oxide:
554 Thermodynamic and Kinetic Study, *Sep. Sci. Technol.*, 46 (2011) 2531-2538.

555 [41] M. Kersten, S. Karabacheva, N. Vlasova, R. Branscheid, K. Schurk, H. Stanjek, Surface
556 complexation modeling of arsenate adsorption by akagenite (β -FeOOH)-dominant granular ferric
557 hydroxide, *Colloid. Surface. A*, 448 (2014) 73-80.

558 [42] S. Wang, H. Lan, H. Liu, J. Qu, Fabrication of FeOOH hollow microboxes for purification of heavy
559 metal-contaminated water, *Phys. Chem. Chem. Phys.*, 18 (2016) 9437-9445.

560 [43] S. Wang, C.N. Mulligan, Occurrence of arsenic contamination in Canada: sources, behavior and
561 distribution, *Sci. Total Environ.*, 366 (2006) 701-721.

562 [44] X. Xie, A. Ellis, Y. Wang, Z. Xie, M. Duan, C. Su, Geochemistry of redox-sensitive elements and
563 sulfur isotopes in the high arsenic groundwater system of Datong Basin, China, *Sci. Total Environ.*, 407
564 (2009) 3823-3835.

565 [45] G. Zhang, H. Liu, R. Liu, J. Qu, Adsorption behavior and mechanism of arsenate at Fe-Mn binary
566 oxide/water interface, *J. Hazard. Mater.*, 168 (2009) 820-825.

567 [46] GAO-SHENG ZHANG, JIU-HUI QU, HUI-JUAN LIU, RUI-PING LIU, G.-T. LI, Removal
568 Mechanism of As(III) by a Novel Fe-Mn Binary Oxide Adsorbent: Oxidation and Sorption, *Environ.*
569 *Sci. Technol.*, 41 (2007) 4613-4619.

570 [47] L. Tang, H. Feng, J. Tang, G. Zeng, Y. Deng, J. Wang, Y. Liu, Y. Zhou, Treatment of arsenic in acid
571 wastewater and river sediment by Fe@Fe₂O₃ nanobunches: The effect of environmental conditions and
572 reaction mechanism, *Water Res.*, 117 (2017) 175-186.

573 [48] KATJA AMSTAETTER, THOMAS BORCH, PHILIP LARESE-CASANOVA, A. KAPPLER,
574 Redox Transformation of Arsenic by Fe(II)-Activated Goethite (α -FeOOH), Environ. Sci. Technol., 44
575 (2010) 102-108.
576